ARMY RESEARCH LABORATORY

Dynamic Fracture of Composite Gun Tubes

by Jerome T. Tzeng

ARL-TR-1869

January 1999

Army Research Laboratory
Aberdeen Proving Ground, MD 21005-5066

ARL-TR-1869 **January 1999**

Dynamic Fracture of Composite Gun Tubes

Jerome T. Tzeng
Weapons and Materials Research Directorate, ARL

Abstract

The fracture behavior of a composite cylinder subjected to a moving pressure has been investigated. The resonance of stress waves can result in very high amplitude of strains in the cylinder at the instant and location of pressure front passage when the velocity of the moving pressure approaches a critical velocity. The stress wave with high magnitude, while short in duration, might not cause structural failure immediately; however, it could accelerate the propagation in the cylinder with initial imperfection and shorten fatigue life of the cylinders. The fracture mechanism induced by dynamic amplification effects is especially critical for composite-overwrapped cylinders because of the multimaterial and anisotropic construction, thermal degradation in material properties, and a design goal that is inherent in lightweight gun barrel applications.

Table of Contents

List of Figures

Figure		Page

1. Introduction

Traditionally, the fatigue cycles of a steel gun tube are calculated based on the frequency of firing with an assumption of a static loading condition. For a lightweight composite gun barrel, fatigue and fracture due to dynamic response of structures has to be considered from design points of view. Cyclic stress and strain generated by the dynamic loads within a firing cycle might significantly accelerate the rate of propagation of an existing crack in the structure. The fracture mechanism under a transient loading condition could be quite different from that produced by relatively static loading. From a material point of view, fracture toughness and strength could change due to loading rates. A reinforced polymer composite might become more brittle if it is loaded at higher strain rate. The fracture toughness and strength measured in static loading conditions might not be suitable for a transient case. In this paper, stress waves due to a dynamic response in a composite-wrapped steel liner are modeled and used to study fracture behavior of gun barrels. A strain-energy integration approach, originally suggested by Rice [1] as J-integral, is then proposed to evaluate crack propagation at the interface of the composite and liner. This paper also discusses how the energy integration can be used to predict the crack propagation in gun barrels from an implementation point of view.

Very high amplitude and frequency strains, commonly referred to as dynamic strain amplification, develop in a cylinder at the passage of the moving pressure front. The phenomenon is caused by the resonance of flexural waves when the moving pressure approaches a critical propagation velocity of the flexural waves in the cylinder. The resonance response of a cylinder, subjected to moving pressure loads, has been investigated by Taylor [2], Jones and Bhuta [3], Tang [4], and Reismann [5]. More recently, Simkins [6] investigated the response of flexural waves in constant cross-sectional tubes, and Hopkins [7] used the finite element method to study the dynamic strain response of a tube with various cross sections. Recently, Tzeng and Hopkins [8] extended the research on the dynamic strain effect to cylinders made of fiber-reinforced composite-overwrapped materials with a metal liner. The results are very applicable to lightweight composite cylinders used for gun tubes and high-pressure piping systems.

The dynamic strain effect is especially critical for composite-overwrapped cylinders that are designed to achieve enhanced performance with relatively light weight. From a design point of view, the weight savings generally decreases the rigidity and inertia of the tubes under dynamic loads. These effects are especially critical for thin-walled cylinders, since local shell bending is caused by the pressure discontinuity as the pressure front travels down the tube. The deformation, due to shell bending, can develop high axial and transverse shear stresses. The transverse shear stress magnitude is critical, since the shear strength of composites is generally much lower than the shear strength of metals. The dynamic analysis is especially critical from the design point of view, since the stress and strain levels can be two to three times higher under dynamic conditions than those attained under static loading conditions. Accordingly, the response at the interface between the composite overwrap and steel liner becomes very important. The shear properties and tensile peel strength at this interface are low, in general, due to relatively poor adhesion between different materials, which might result in an initial debonding. The dynamic cyclic strains from oscillation may cause crack propagation of the composite materials and eventually lead to fracture of the overwrapped cylinder.

2. Analysis

In this section, the dynamic response and fracture of a composite-overwrapped cylinder subjected to a moving pressure are investigated by using both analytical and numerical methods. As a first approximation, Love's thin-shell theory is used to derive a closed-form expression for the critical velocity. The critical velocity at which resonance occurs is greatly influenced by tube geometry and material properties. The finite element solution is obtained using a version of the DYNA2D [9] hydrocode, which has been modified to allow accurate modeling of the moving- pressure front. This approach allows modeling of both the moving-pressure front and the composite cylinder geometry with initial cracks in sufficient detail to simulate the actual loading conditions. Finally, an integration of strain energy density along a specific path within a cylinder is presented and used as an indication for crack propagation.

2.1 Fracture and Energy Density Integration. Consider a crack at the interface of the composite overwrap and steel liner as shown in Figure 1. The strain fields near the crack tip are difficult to determine, especially in this bimaterial system with anisotropy of composite laminates. With the assumption that the crack at the interface is axisymmetric, analysis can be done by a two-dimensional model both for the far-field analysis and the crack tip. Rice [1] proposed the J-integral method, which bypasses the complexity of solving a boundary value problem. An integral surrounding the crack tip with a path of Γ can be defined as

$$J = \int_{\tau} \left(\omega \, dy - \vec{T} \cdot \frac{\partial \vec{u}}{\partial x} ds \right) + \int_{v} \left(\rho \dot{u} \frac{\partial \dot{u}}{\partial x} \right) dV, \tag{1}$$

where ω is the strain energy density and can be defined as

$$\omega = \omega(\epsilon) = \int_0^{\epsilon} \sigma_{ij} \, d\epsilon_{ij}. \tag{2}$$

T is the traction vector along the path, u represents the displacement vectors, ds is an element of arc length along Γ, and V is volume.

Kinetic energy associated with the internal movement of material is neglected at the moment; however, the effects are shown in equation (1) by Atluri [10] and Doyle and Farris [11]. As pointed out by Rice [1], the J-integral is equivalent to strain energy release rate at the crack for an elastic case that results in the following expression:

$$J = -\frac{\partial V}{\partial a} = G = G_I + G_{II} + G_{III}, \tag{3}$$

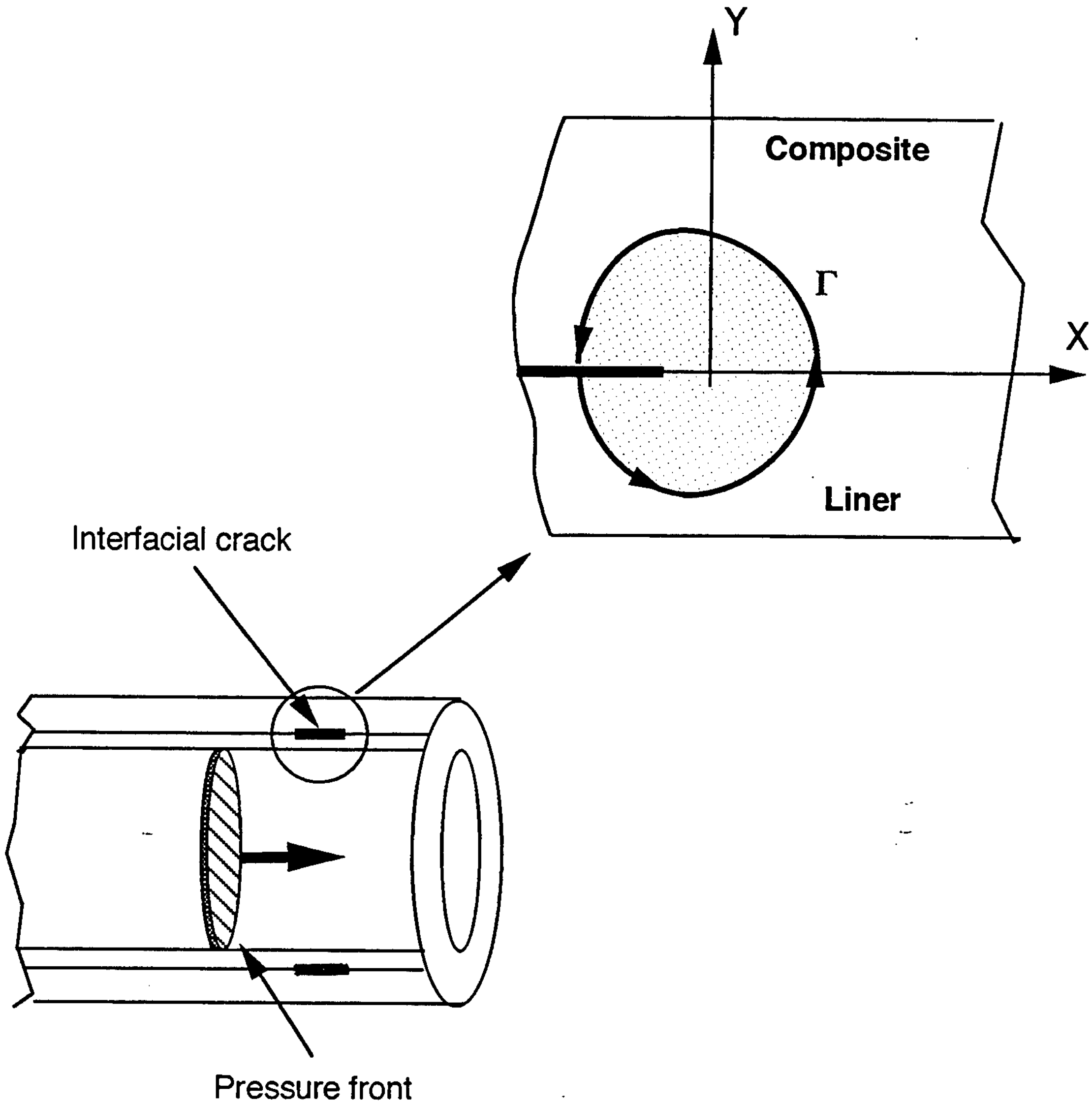

Figure 1. An Integration Around a Crack at the Interface of Composite and Metal Liner.

where V represents the potential energy of an elastic body, a is a crack length in the body, and G is the total strain energy release rate resulting from three fracture modes. Accordingly, the strain energy release rate is related to stress intensity as follows:

$$G = \frac{1 - \nu^2}{E}\left(K_I^2 + K_{II}^2 + \frac{K_{III}^2}{1 - \nu}\right), \tag{4}$$

where K_I, K_{II}, and K_{III} are stress intensity factors associated to different modes, and the analysis is assumed to be a plane strain case.

The integration of strain energy can be carried out with an implementation of a finite element technique. A composite-overwrapped cylinder with an initial crack at the composite/liner interface can be modeled in detail. Stress and strain fields in the region surrounding the crack can be obtained through a transient analysis. Strain energy density and its integration are then calculated element by element through a specific path. The results will then be ready for comparison with empirical data and serve as a useful design and fabrication parameter.

2.2 Dynamic Response of Cylinders. The critical velocity of a flexural wave in a cylindrical tube can be obtained from Love's thin-shell theory. The closed-form solution is valuable in illustrating and understanding the important parameters that determine the dynamic response of the cylinder. The results can also be compared with the critical velocity values obtained using finite element techniques. The finite element values will approach the exact solution as the mesh discretization increases. Consider a thin, orthotropic cylinder of radius R subjected to a transient axisymmetric radial load (e.g., a moving internal pressure, P). Figure 2 shows the geometry, coordinate system, and pressure loading condition being considered. The governing equation for this model with a moving internal pressure front, expressed as Heaviside step function, can be shown to be given by

$$m\frac{\partial^2 W}{\partial t^2} + D_x\frac{\partial^4 W}{\partial x^4} + \frac{12\,(1 - \nu_{\theta x}\nu_{x\theta})}{h^2 R^2} D_\theta W = P(1 - H(x - Vt)), \tag{5}$$

where W is the radical displacement dependent upon time, t, and axial position coordinate, x; m is the mass, which is equal to ρh; ρ is the density of shell material; h is the thickness of the shell; P is the internal pressure; and V is the pressure front velocity, which is assumed constant. The shell-bending stiffness in the axial and circumferential directions is in equations (6) and (7), respectively.

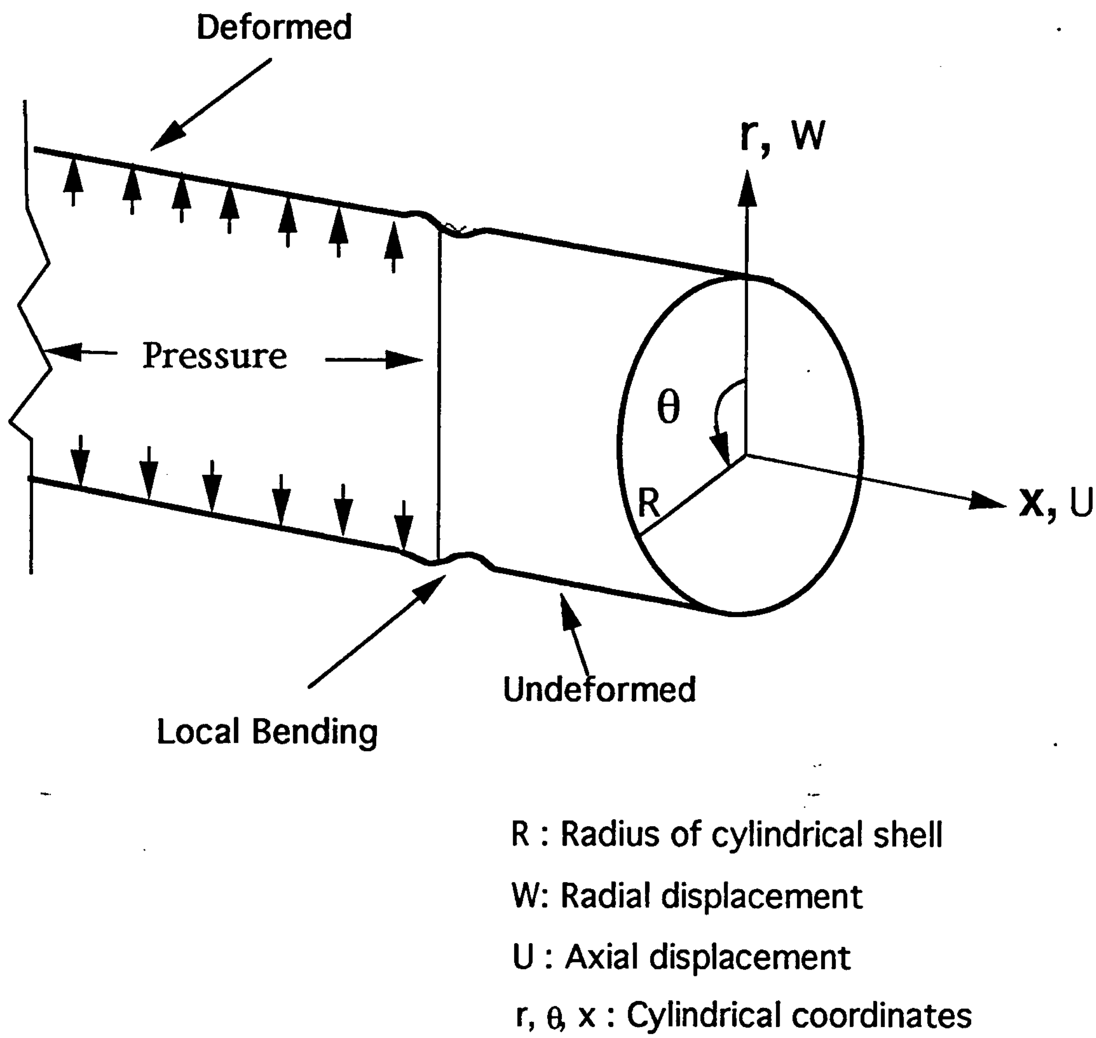

Figure 2. Deformation and Coordinates Definition of Cylindrical Shell Subjected to a Moving Pressure.

$$D_x = \frac{E_x h^3}{12(1 - \nu_{\theta x}\nu_{x\theta})}, \tag{6}$$

and

$$D_\theta = \frac{E_\theta h^3}{12(1 - \nu_{\theta x}\nu_{x\theta})}, \tag{7}$$

where E_x and E_θ are the effective (smeared) elastic moduli, and $\nu_{x\theta}$ and $\nu_{\theta x}$ are the effective Poisson's ratios of the composite material in the axial and circumferential directions, respectively. For a composite tube with cross-ply laminate construction, the shell-bending stiffness is different in the axial and circumferential directions and is determined by the axial-to-hoop layer ratio. The loading function, $P\,(1-H(x-V_t))$ in equation (5), represents the internal pressure front traveling in the axial direction with constant velocity V. $H(x-Vt)$ is the Heaviside step function. Accordingly,

$$
\begin{aligned}
P\,(1 - H(x - Vt)) &= 0 \text{ when } x > Vt \\
&= P \text{ when } x \le Vt.
\end{aligned}
\tag{8}
$$

The critical velocity for an orthotropic cylindrical shell, derived from the characteristic function obtained from equation (5) is given by

$$
V^2_{cr,\,comp} = \sqrt{\frac{1}{3(1 - \nu_{\theta x}\nu_{x\theta})}}\left(\frac{h}{R}\right)\left(\frac{\sqrt{E_\theta E_x}}{\rho}\right).
\tag{9}
$$

Equation (9) clearly shows that the critical velocity of an orthotropic cylinder subjected to a moving-pressure front is a function of the tube's geometry, density, Poisson's ratios, and elastic moduli. The critical velocity increases when either of the elastic moduli increases, as well as when the shell thickness-to-radius ratio increases. From a design point of view, a tube constructed with high stiffness and lightweight materials is preferred for dynamic loading conditions. However, equation (9) indicates that a larger wall thickness is required, in general, for the tube geometry when a high-velocity pressure front is present, if the rest of the parameters are kept for the same. However, it also shows that both axial and hoop moduli (i.e., E_θ and E_x) have influence on the critical velocity. Accordingly, the design optimization can be achieved by varying the laminate architecture of composite cylinders.

For an isotropic region, equations (5)–(9) can be greatly reduced and simplified since the material properties are the same in hoop and axial directions (i.e., $D_\theta = D_x$, $E_\theta = E_x$, and $\nu_{\theta x} = \nu_{\theta x}$). Accordingly, the critical velocity can be expressed as

$$V^2_{cr,comp} = \sqrt{\frac{1}{3(1-\nu^2)}}\left(\frac{h}{R}\right)\left(\frac{E}{\rho}\right). \tag{10}$$

2.3 Finite Element Modeling. The closed-form solution described in section 2.1 can be applied accurately to a cylindrical shell under the assumption of infinite length. For a finite length cylinder with varying cross-sectional area along its length and multimaterial construction, the finite element method allows for a more expedient and straightforward procedure for determining the critical velocity. A hydrodynamic finite element code, DYNA2D, was modified to simulate the moving-pressure boundary condition. As shown in Figure 1, a slideline that allows a dummy material block to move freely along the axial direction of the cylinder is included in the finite element model of the cylinder. The instantaneous location of the pressure front is then easily determined by tracking the location of the rear face of the dummy material block. To accurately capture the oscillatory dynamic response of the tube, the computation is carried out with a very small time interval (~10^{-6} s). This time interval also allows the pressure to slowly ramp to a maximum value as element surfaces are uncovered by the moving block. This means that artificial numerical stress oscillations, due to the sudden application of the pressure boundary condition on an element face, are minimized so that these numerical oscillations do not adversely affect the solution. While for the cases examined in this study the velocity was held constant, the methodology can also be used to simulate the effect of an accelerating pressure front, if desired.

Since the composite tube has a laminated construction, ideally, a ply-by-ply model will yield the best result and accuracy. However, this would dictate the use of many thousands of elements in the a finite element model. This level of detail, coupled with the very short time step interval required for a dynamic analysis, would lead to an unreasonably long computational time. Also, an additional potential side effect of taking many millions of time steps would be to potentially induce numerical instabilities due to round-off errors. Avoiding these constraints thus limits the size (e.g., number of elements) of the finite element model that can be analyzed within a reasonable computational time. In composite analysis, it is standard practice to use smeared properties for the composite laminate. These properties, which are representative of the unique lay-up construction of the tube, were calculated using a model developed by Alexander and Tzeng [12]. The smeared property approach allows a single finite element to contain several layers. Accordingly, the size of the finite element model can be greatly reduced.

3. Results

The cylinder used in this analysis is 100 in long with a constant wall thickness. The steel liner and composite overwrap are 0.075 in and 0.125 in thick, respectively. The smeared properties for a composite tube composed of 25% axial (x-direction) and 75% hoop (θ-direction) plies are shown in Figure 3. The properties are calculated based on the use of an IM7 graphite/8551-7 epoxy composite. The unit ply properties are also given in Figure 3. The cylinder is equally divided into 400 elements along the axial direction and 10 elements through the wall thickness. There are four elements representing the steel liner and six elements representing the composite overwrap. In all, the model contains 4,000 elements. The cylinder is subjected to a moving internal pressure of 6,000 psi.

3.1 Velocity Effects of Moving Pressure. Two pressure front velocities, a subcritical velocity of 2,500 ft/s (case 1) and a supercritical velocity of 3,500 ft/s (case 2), are performed to demonstrate the dynamic effects. The total time for the pressure front to traverse down the tube was about 3.33 and 2.43 ms for cases 1 and 2, respectively. The time increment used in the analysis was on the order of 1 μ; therefore, approximately 3,500–4,000 time steps were used per analysis. The finite element models, including the composite cylinder and the dummy material block, are shown in Figure 4 at a time instant when the block was traveling 20 in from the initial position. The block is then given an initial velocity, which is held constant throughout the analysis. Finally, because an axisymmetric model was employed, only one-half of the cylinder is shown.

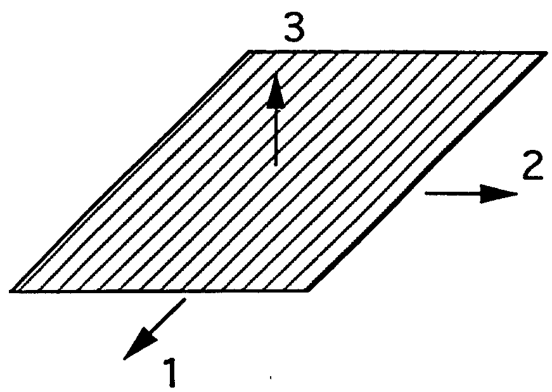

$E_{11} = 25.0E+06$ $\quad G_{12} = 7.0E+05$

$E_{22} = 1.2\ E+06$ $\quad G_{13} = 7.0E+05$

$E_{33} = 1.2\ E+06$ $\quad G_{23} = 5.3E+05$

$\nu_{12} = 0.33$ $\quad \nu_{23} = 0.31$

$\nu_{13} = 0.33$

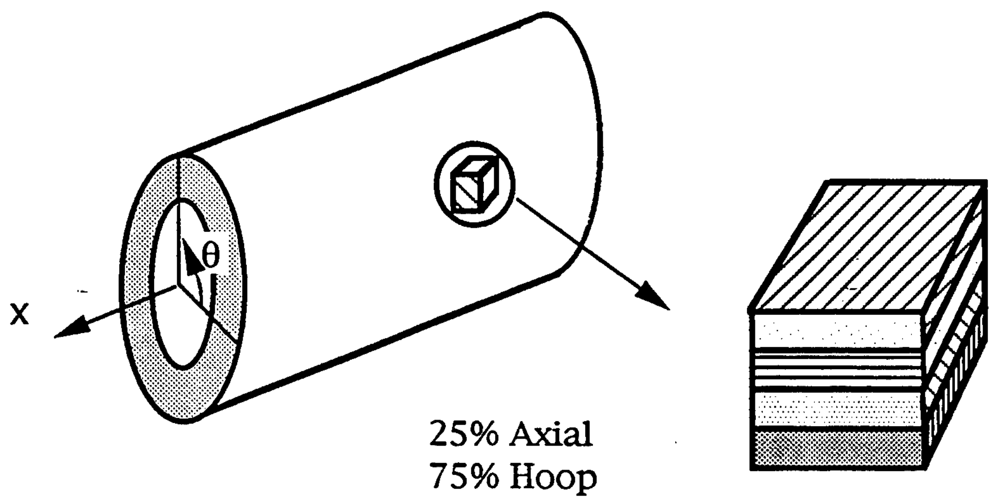

$E_r = 1.298E+06$ $\quad G_{rx} = 4.095E+05$

$E_x = 7.214E+06$ $\quad G_{\theta r} = 4.610E+05$

$E_\theta = 19.10E+06$ $\quad G_{\theta x} = 7.000E+05$

$\nu_{\theta r} = 0.3825$ $\quad \nu_{xr} = 0.338$

$\nu_{\theta x} = 0.0556$

Figure 3. Smeared Properties of the Composite Tube.

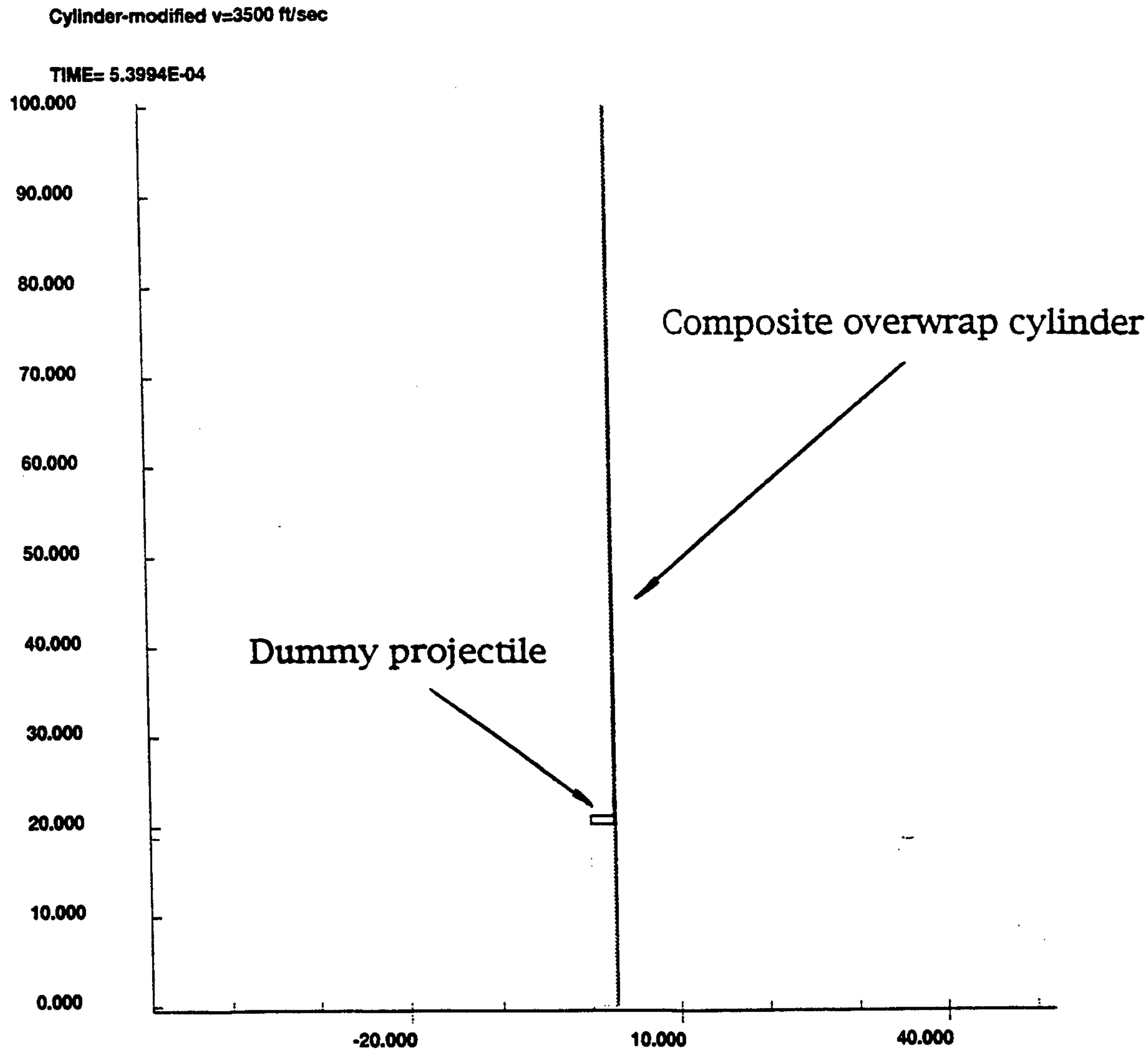

Figure 4. Finite Element Model of the Composite-Overwrapped Cylinder With the Dummy Projectile at Time = 5.3994 E−4 s.

A fringe plot of the radial displacement in the neighborhood of the projectile with velocity of 3,500 ft/s at this specific instant is shown in Figure 5. The fringe pattern clearly shows the stress oscillation, due to induced-bending boundary layer stresses in the wall of the cylinder as it is subjected to a moving-pressure front. There are no strain and stress waves occurring at a low velocity. The maximum displacement is located very close to the pressure front where pressure discontinuity is located. The displacement then decreases with increasing axial distance from the location of the pressure front discontinuity. The deformation is transient and cyclic with time and position.

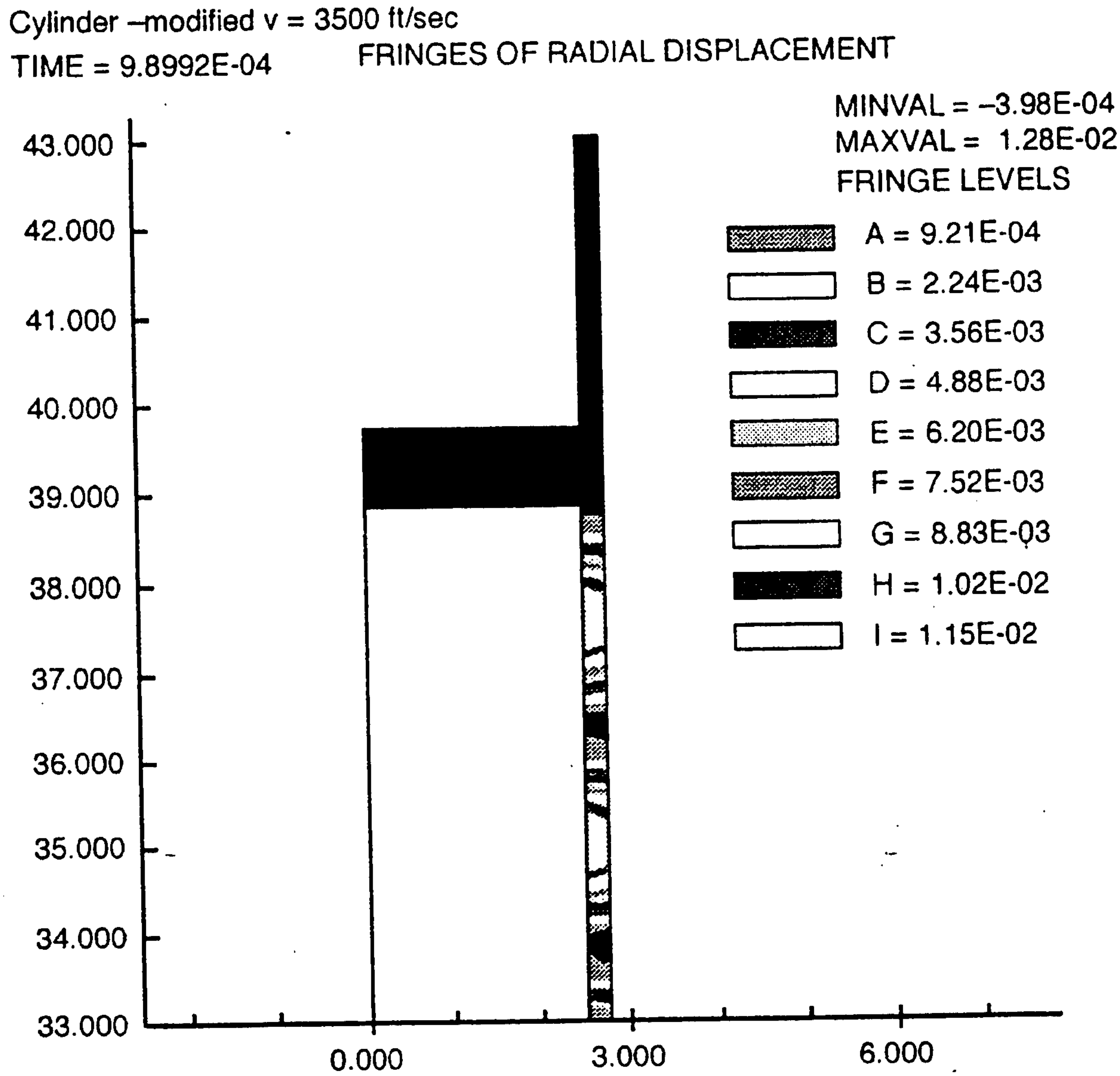

Figure 5. Radial Displacement in the Vicinity of the Projectile Passage at Time = 5.3994 E−4 s.

The way of presenting the data described previously can clearly illustrate the spatial variation of the displacement and, consequently, strain and stress fields. This view corresponds to what observers traveling with the pressure front see as they pass through the cylinder. An alternate view is to pick a fixed location on the tube and observe the change in displacement as the pressure front approaches this position and then passes it (using a time history plot for a given location). This corresponds to what is measured with strain gauges or accelerometers attached to the tube. The radial locations at which various displacement and stress components are examined in this paper are shown in Figure 6. These radial locations represent positions at which these displacement and stress

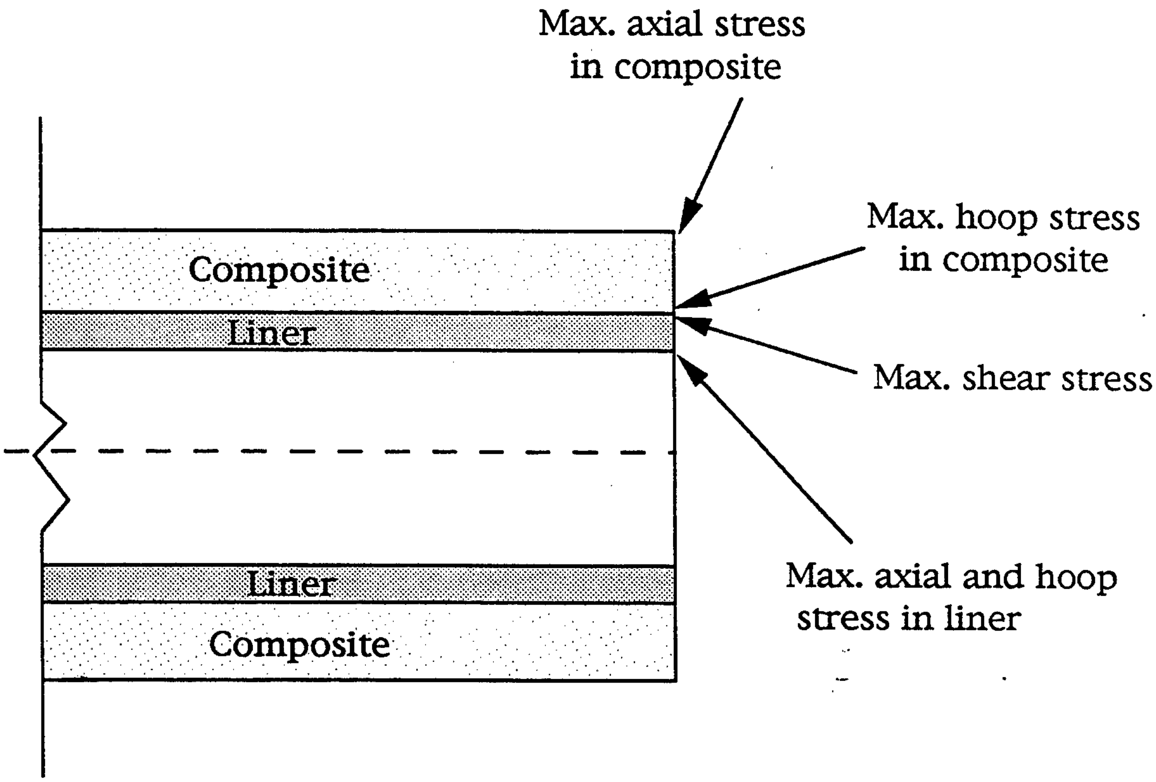

Figure 6. Locations of the Maximum Stress Components.

components attain their greatest values as discussed in detail next. Since the tube is subjected to an internal pressure, the maximum hoop stress occurs at the inner surface of the liner. As the pressure front passes a given axial location, a local axisymmetric bending occurs in the tube wall. The maximum axial stress will thus occur at the innermost surface of the liner and the outermost surface of the composite. The maximum shear stress associated with the bending is located at the neutral cross section. Accordingly, the critical value of the shear stress in the transverse direction of composite laminate occurs near the interface of the liner and the composite overwrap. Figures 7–10 plot the various displacement and stress component vs. time at these locations for the cylinder.

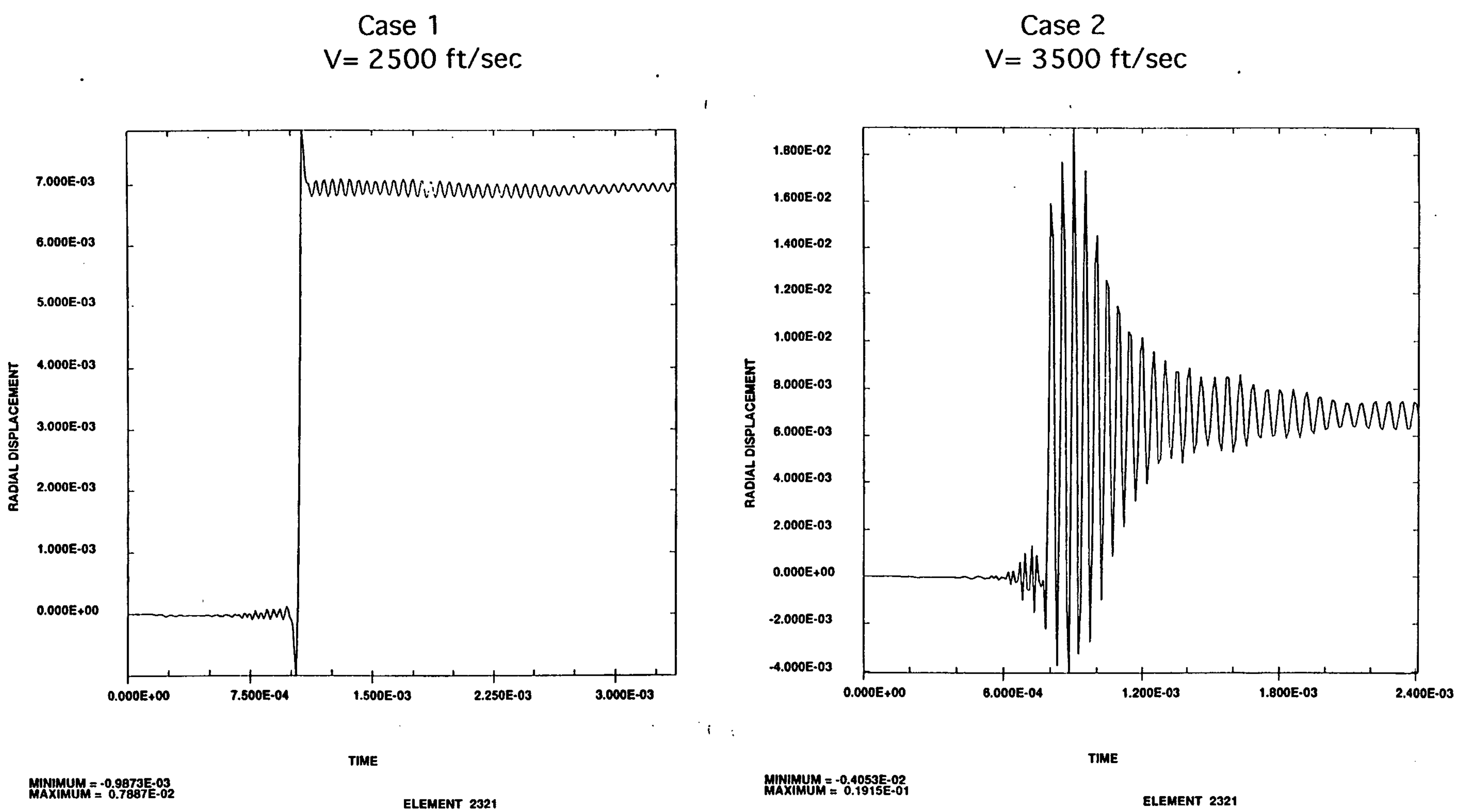

Figure 7. Radial Displacement in the Innermost Region of the Composite Overwrap.

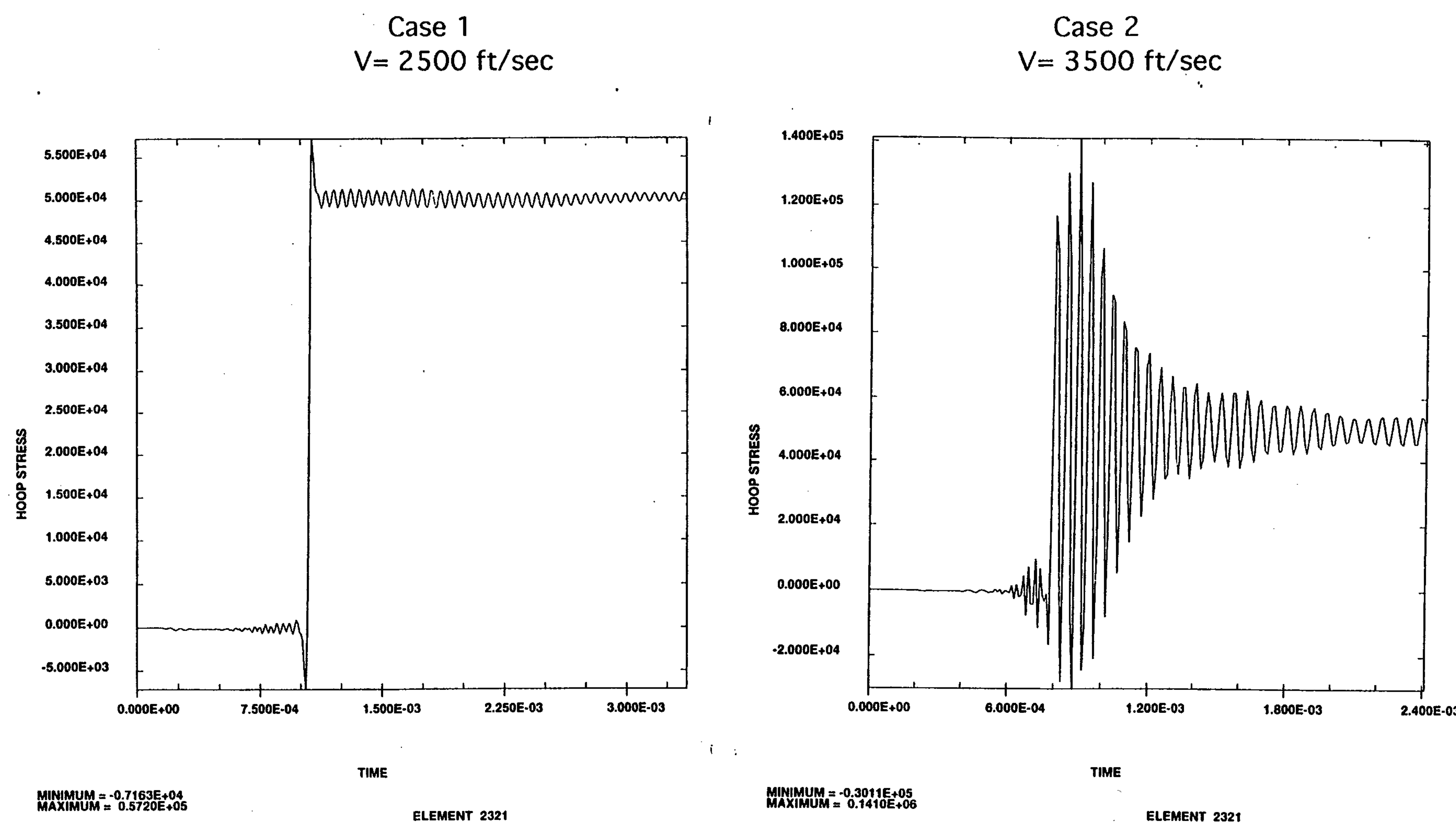

Figure 8. Hoop Stress in the Innermost Region of the Composite Overwrap.

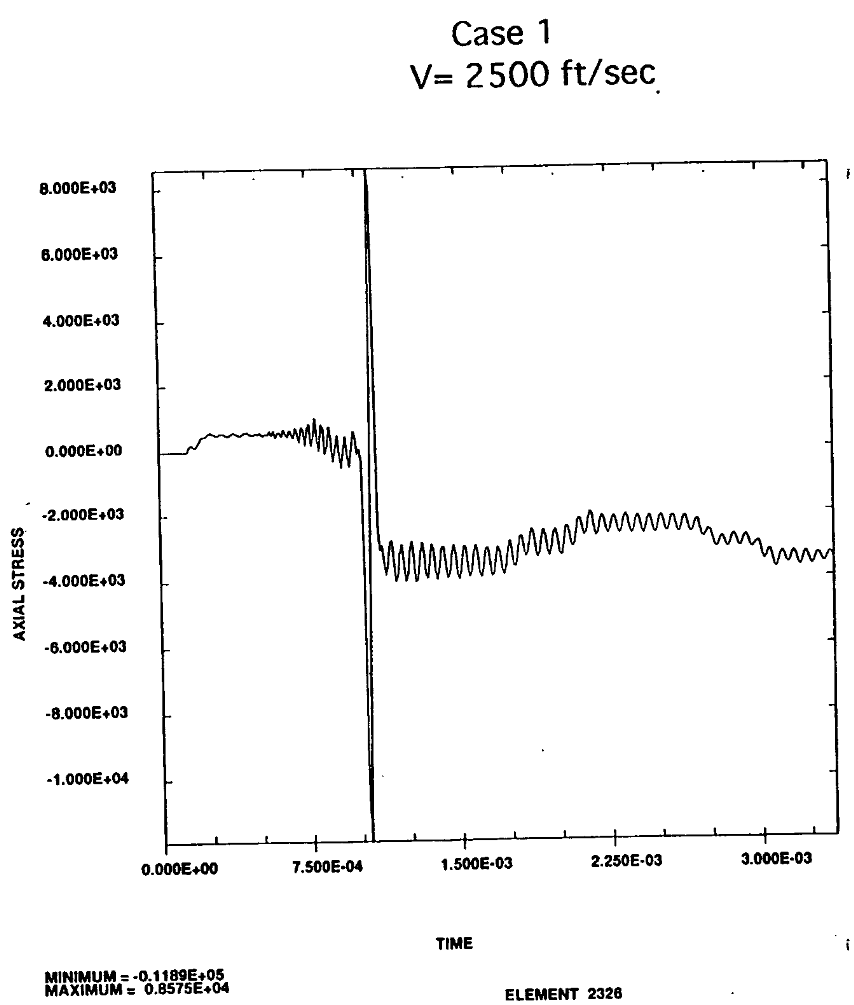

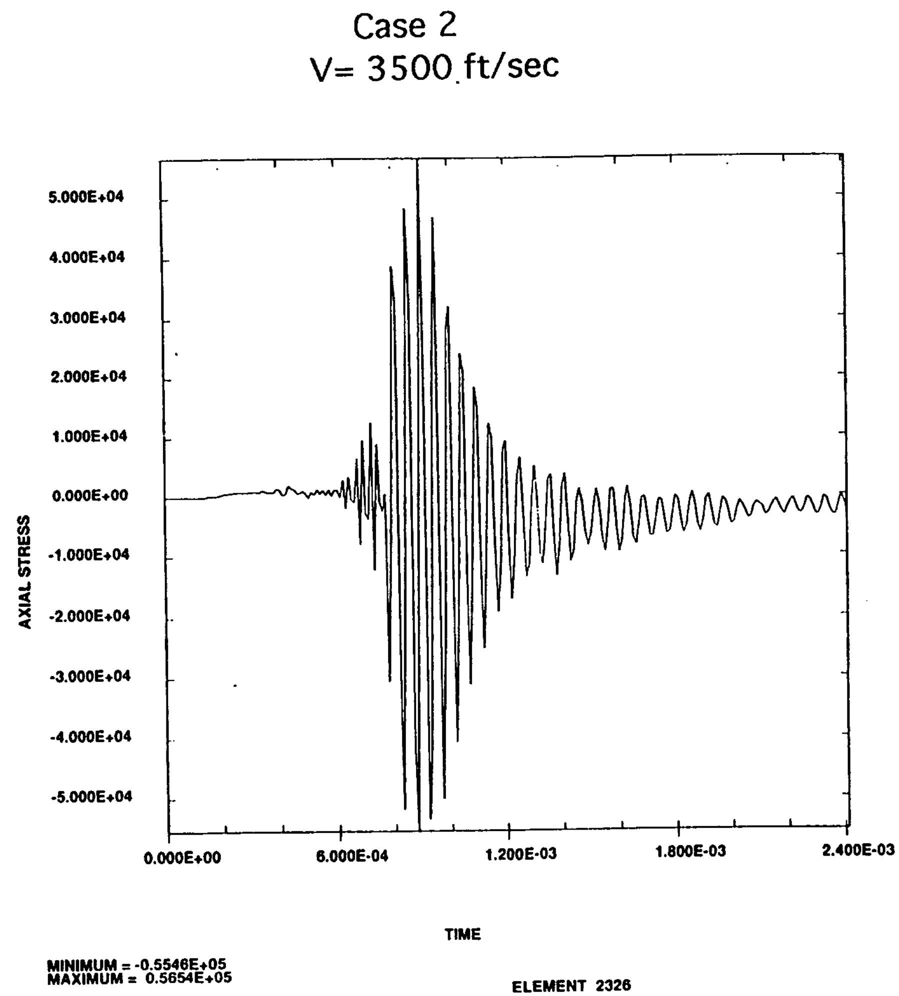

Figure 9. Axial Stress in the Outermost Region of the Composite Overwrap.

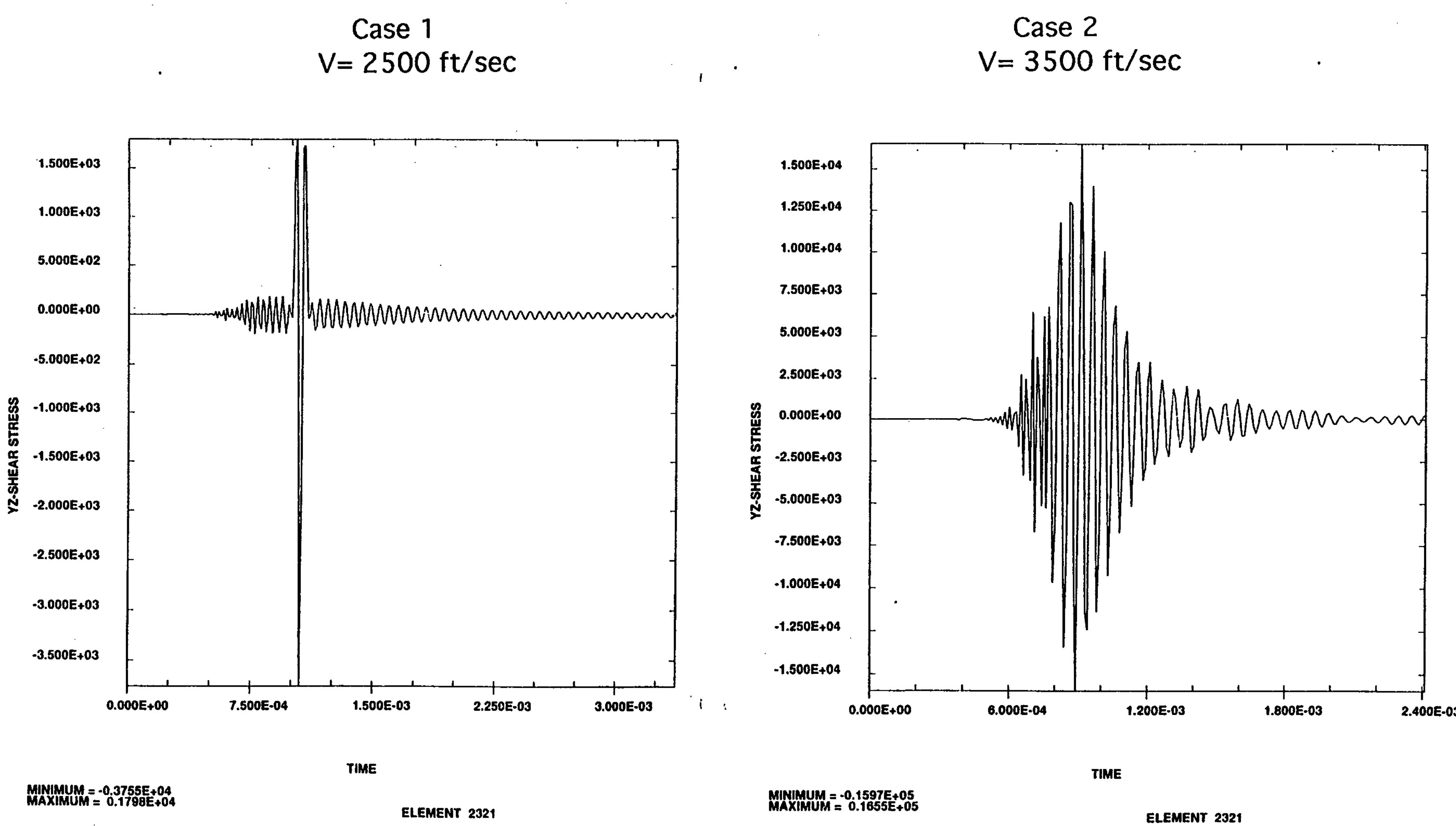

Figure 10. Interlaminate Shear Stress in the Innermost Region of the Composite Overwrap.

The radial displacement at the innermost region of the composite in Figure 7 shows a dramatic difference in the magnitude of peak displacements, as well as in temporal behavior of the oscillations as the projectile velocity changes, case 1 vs. case 2. Before the arrival of the pressure front, the cylinder at these observed locations is basically undeformed. The small oscillations that occur just before projectile arrival are real and represent stress oscillations, due to the moving-pressure front. Similar behavior is predicted by thin-wall shell theory. It is seen that at the instant the pressure front passes, the radial displacement undergoes a rapid increase. However, for sufficiently low velocities, similar to case 1, the displacement and stresses are still close to what would be predicted based upon Lame's equation for a static internal pressure loading. This is not the case, though, for velocities near or above the critical velocity shown in Figure 7, case 2. A very large radial displacement occurs for this case where the pressure front velocity is 3,500 ft/s. In fact, this velocity exceeds the critical velocity of the composite-overwrapped cylinder. The peak magnitude of the radial displacement is seen to be about 1.5 times the peak magnitude of the radial displacement of case 1, where the velocity is only 2,500 ft/s. As the projectile moves farther away from the axial location, the radial displacement approaches the same magnitude ($\sim 7.5 \times 10^{-3}$ in), as would be predicted by a static analysis of a pressurized tube. This is shown to be true for both case 1 and case 2. It is very important to realize that because the velocity for case 2 is above the critical velocity, the peak radial displacement value is actually less than the peak value that would be obtained if the pressure front had accelerated from 2,500 ft/s to 3,500 ft/s, since, in this scenario, the pressure front would have passed through the critical velocity at some axial location. This would have resulted in a resonant condition at that location, and the peak radial displacement would have been at least twice the Lame's prediction. In fact, theoretically, for linear elastic behavior, the response would have been infinite. This means that the material response would have been limited only by the internal damping of the material coupled with its behavior after yield.

Figure 8 shows the smeared hoop stress induced at the innermost region of the composite. The composite overwrap is constructed with 75% hoop and 25% axial plies, and the smeared hoop stress is, in some sense, the average value for a small representative volume of the laminate at this location. A simple rule-of-mixtures calculation indicated that the peak unsmeared fiber stress in the hoop direction is about 76 ksi for the low-velocity case and 186 ksi for the high-velocity case. The effect of resonance, due to a fast moving-pressure front, is, again, clearly indicated. Figure 9 shows the smeared axial stress at the outermost radius of the composite overwrap. The computed fiber stress is approximately 47 ksi and 220 ksi for the low- and high-velocity cases, respectively; again, this is based on a simple rule-of-mixtures approach. Figure 10 shows the shear stress (t_{rz}) at the innermost radius of the composite overwrap, which is near the neutral axis of the combined steel/composite tube. The shear stress is in the transverse direction of the laminate. The stress levels are 3.7 ksi and 16.5 ksi for the low- and high-velocity cases, respectively. Considering manufacturing factors and the low adhesion strength at the steel/composite interface, the 16.5-ksi shear stress indicates a low margin-of-safety factor.

3.2 Cylinders With an Initial Crack. An initial delamination at the interface of the composite overwrap and steel liner is modeled by adding a slideline into the finite element model developed previously. It is also assumed that there is no friction at the sliding interface. Due to singularity, the stress and strain fields are not accurate in the very near region of the crack tip. Nonetheless, the far-field stress and strain are reasonably accurate and can be used to calculate strain energy density surrounding the crack. Accordingly, a superfine finite element mesh is not necessary if the dynamic response can be fully modeled.

Figure 11 illustrates the finite element model near the crack tip and the path of integration. The path is chosen to be along the coordinate axes to reduce computational efforts. It is also traction-free along the path, which furthermore reduces the complexity of the calculation. The integration can be performed element by element along the path. The strain energy density is calculated at the center of each element and assumed to be uniform in each element. As the density of finite element model increase, the integration will approach an exact solution.

The integration of strain energy density is conservative or path-independent. Theoretically, if there is no crack existing, the integration along any closed loop will be equal to zero. This can be verified numerically by integrating strain energy density along a closed loop, using the results from the previous finite element analysis. For a case with cracks, the stress and strain fields surrounding the crack are no longer the same as those calculated from a model without cracks. Accordingly, the

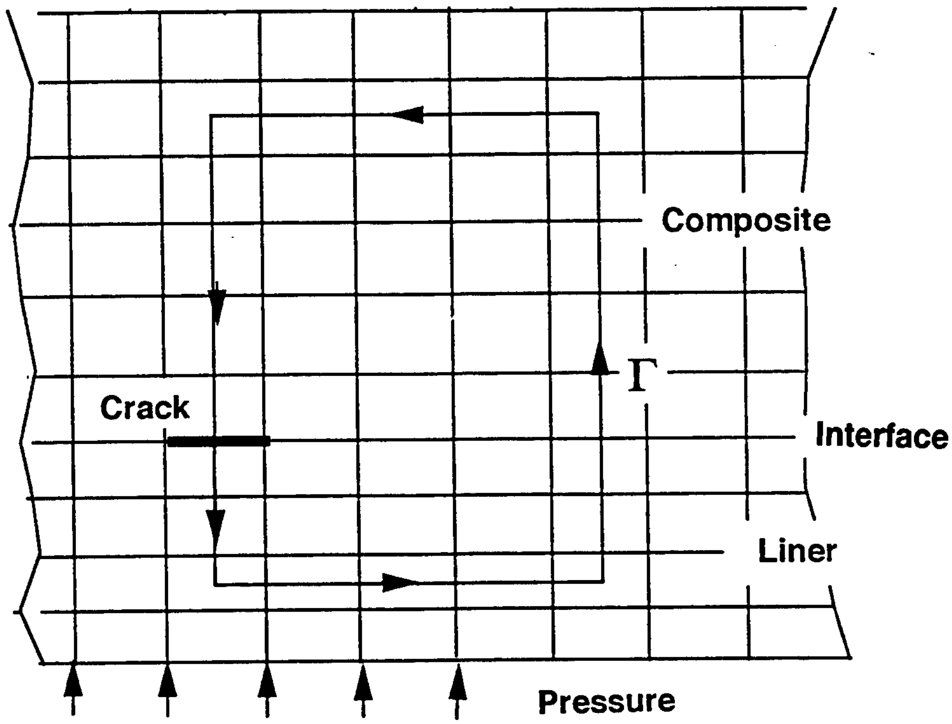

Figure 11. Cylinder With an Initial Crack and an Integration Path.

integration of strain energy density with path will yield to the energy release rate of the specific crack. Furthermore, the integrated energy release rate is determined by the size of crack if the velocity of the pressure front and internal pressure are kept to be a constant.

An analysis was performed for a model with a crack size of 0.75 in along the interface of composite and liner, which is large enough to cause failure of the cylinder by a rapid crack propagation. The internal pressure is about 6,000 psi, and the velocity of pressure front is 3,500 ft/s. Figures 12–15 and Figures 16–19 illustrate strain and stress components, respectively, in a steel element near the crack. Both the stress and strain distributions are quite different from those calculated from a model without cracks due to a stress concentration near the crack.

Equation (1) indicates that integration of strain energy along a cross-loop path around a crack yields the strain energy release rate. A detail of a finite element model near the crack area is shown in Figure 20. A crack or delamination is modeled by placing a sliding interface between elements 484 and 2321. The integration path is shown as the dash linewidth—a counterclockwise loop around the crack. The stress and strain components of each element are then integrated along the path. A

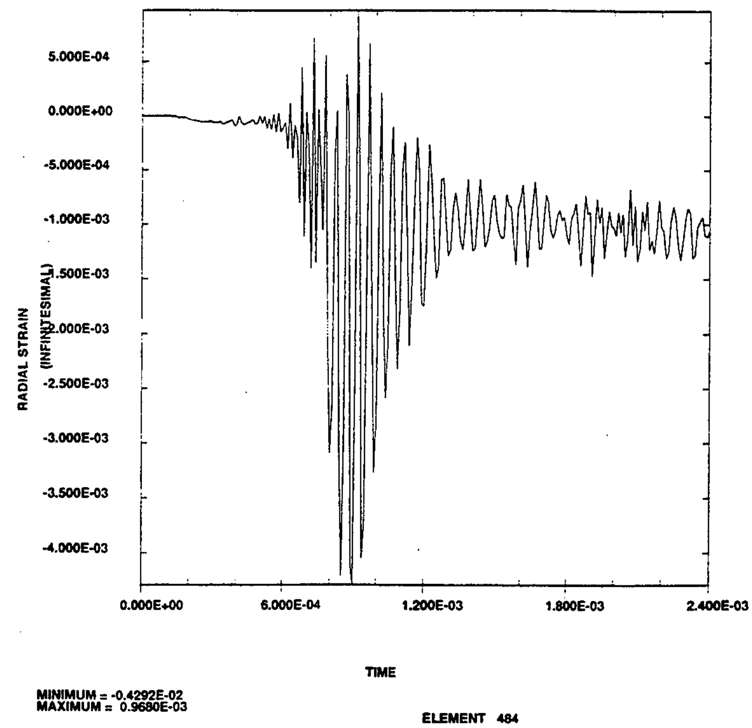

Figure 12. Radial Strain in the Steel Liner Near the Crack.

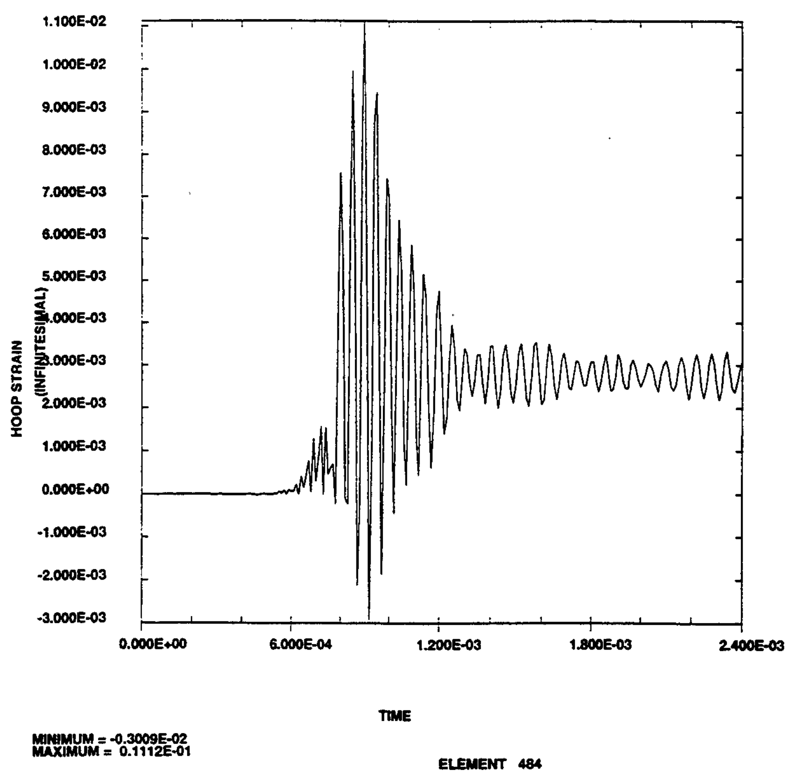

Figure 13. Hoop Strain in the Steel Liner Near the Crack.

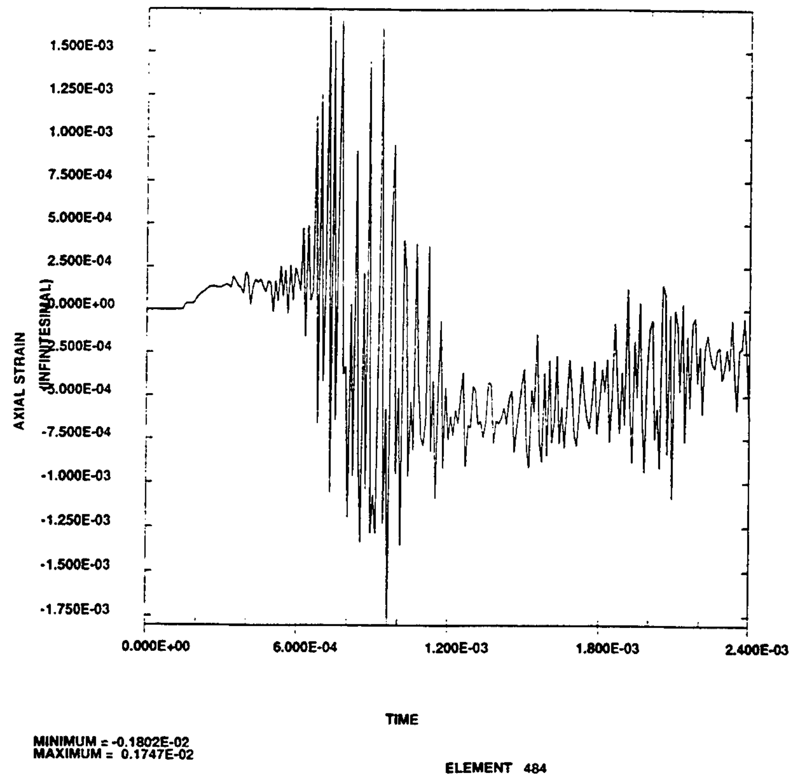

Figure 14. Axial Strain in the Steel Liner Near the Crack.

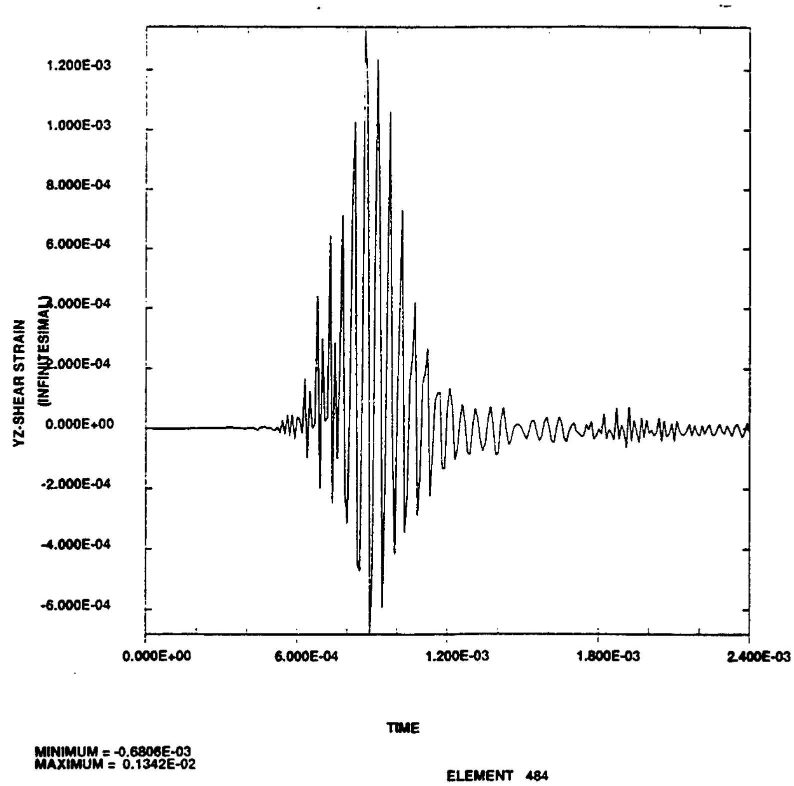

Figure 15. Shear Strain in the Steel Liner Near the Crack.

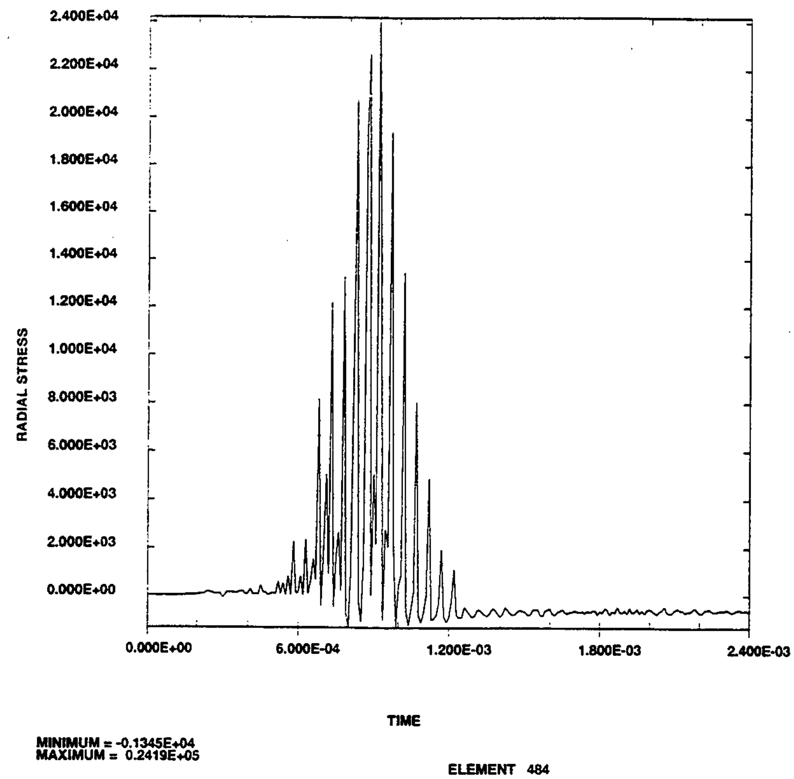

Figure 16. Radial Stress in the Steel Liner Near the Crack.

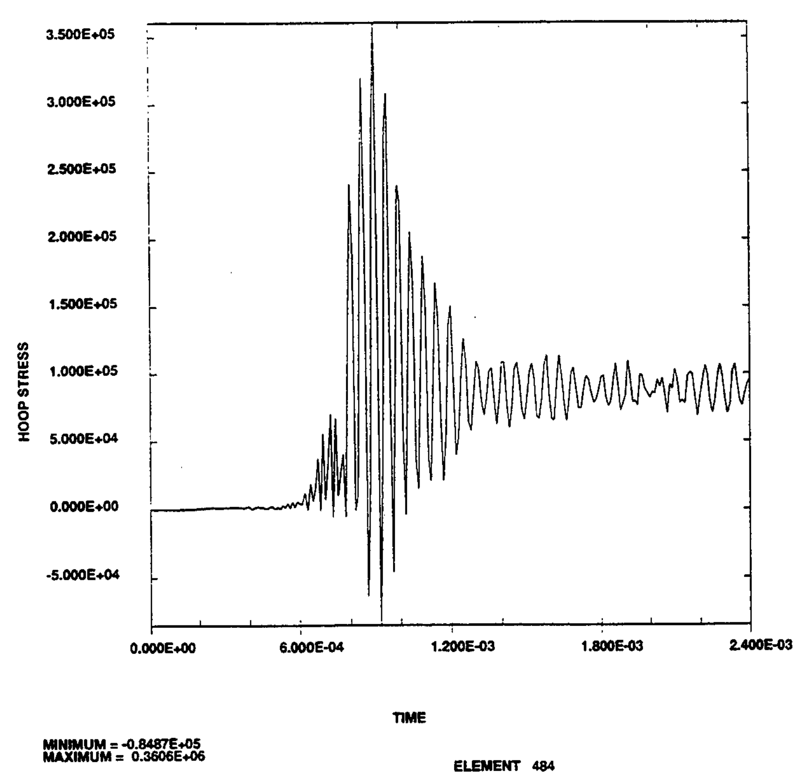

Figure 17. Hoop Stress in the Steel Liner Near the Crack.

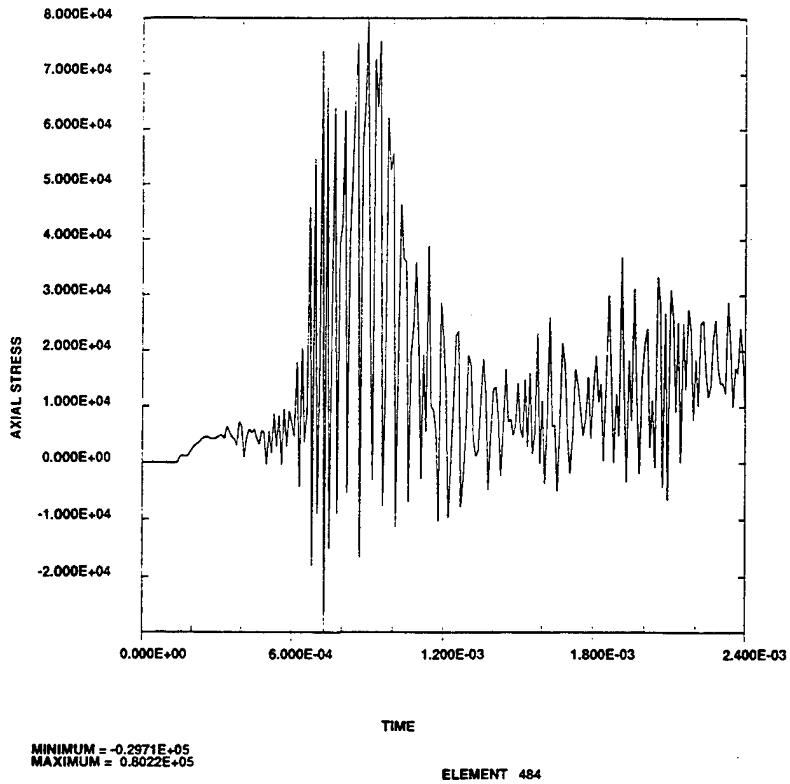

Figure 18. Axial Stress in the Steel Liner Near the Crack.

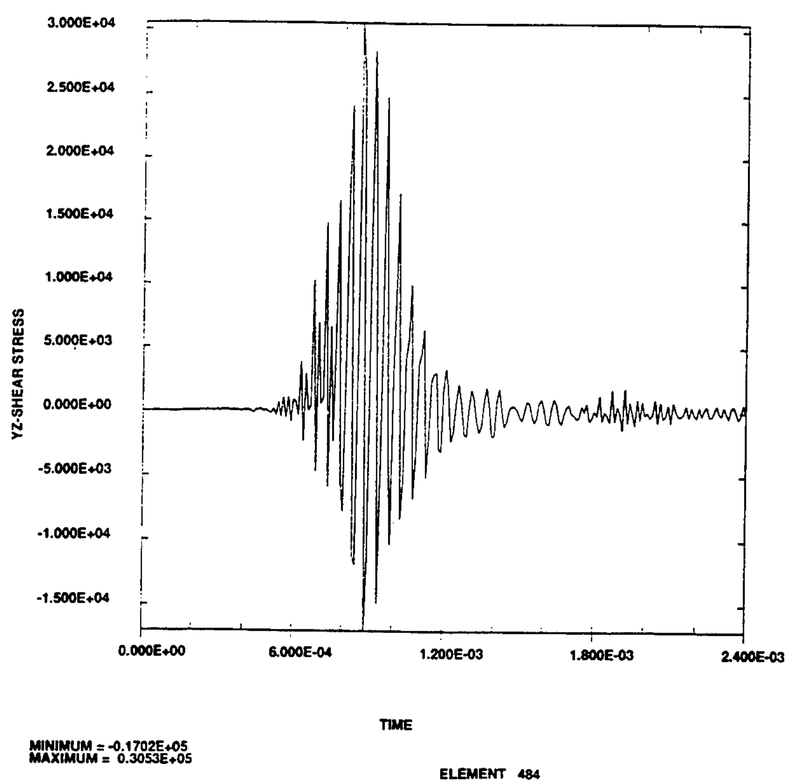

Figure 19. Shear Stress in the Steel Liner Near the Crack.

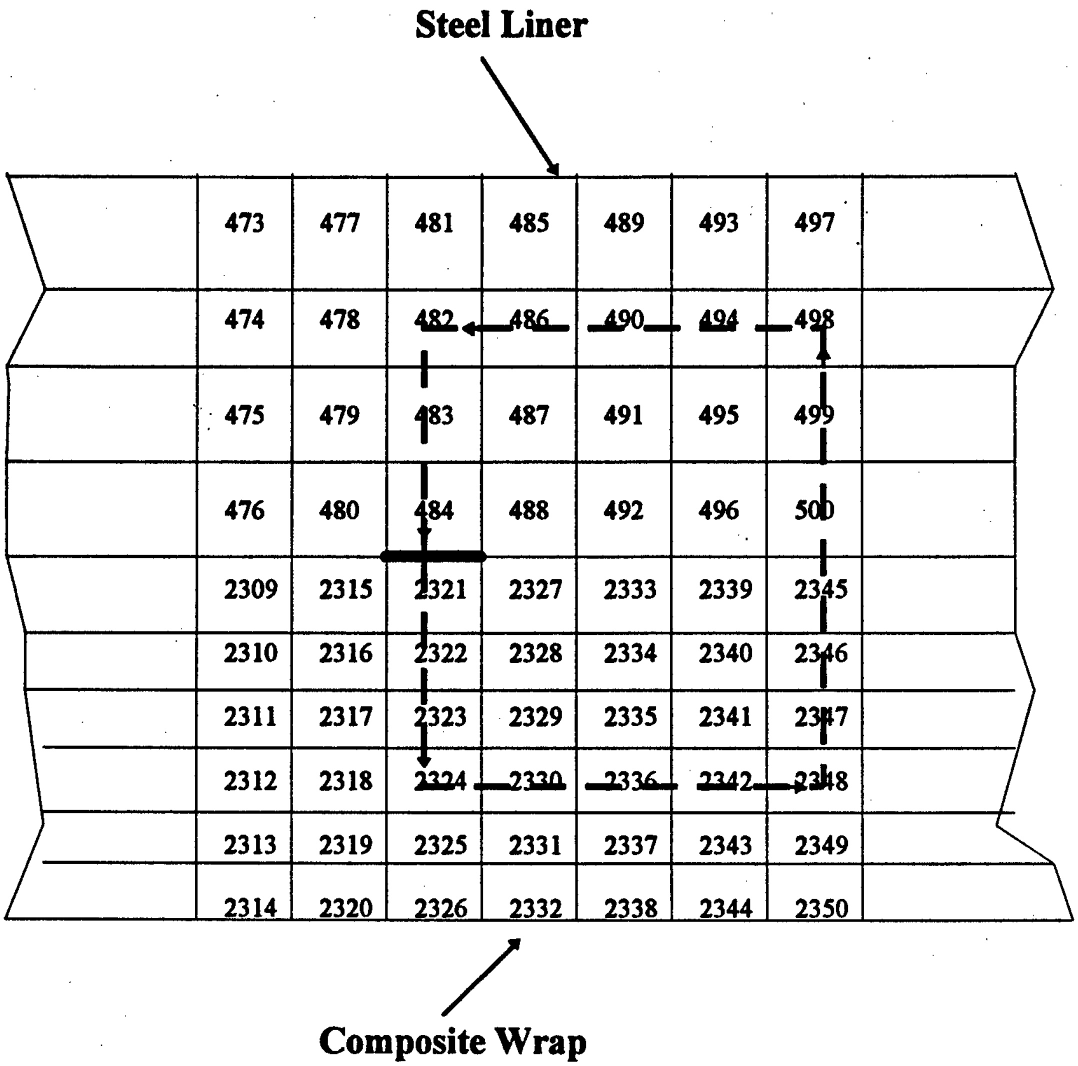

Figure 20. FEM Model and Integration Loop Near the Crack.

combined energy release rate of mode I and II can be calculated from strain energy resulting from radial, axial, and through thickness shear components as

$$G = G_I + G_{II} = 0.01 \text{ ksi-in.}$$

The elastic modulus of the epoxy interface is about 500 ksi; accordingly, we can get the combined toughness from equation (4) as follows:

$$K = \sqrt{K_I^2 + K_{II}^2} \approx 5.0 \text{ ksi-in}^{1/2}. \tag{11}$$

The mode III toughness is not included, since there is no contribution of inplane shear components. It is noted that the computed combined stress intensity, K, is much larger than the fracture toughness measured under a static condition. The K_{1c} is about 1.2 ksi-in$^{1/2}$, and K_{2c} is about 1.5 ksi-in$^{1/2}$ for toughened epoxy. The dynamic fracture toughness will be lower as loading rate increases. Currently, experiments are being conducted to measure dynamic toughness for selected materials. The proposed method does need to be verified with sufficient data in order to be implemented in this specific application.

4. Conclusions

The dynamic analysis of a composite-overwrapped tube illustrates that high-magnitude strains and stresses develop in the cylinder at the pressure front that traverses along the length of the cylinder. The high magnitudes are caused by a resonance condition of the flexural wave propagation with the moving-pressure front velocity. This dynamic strain effect can potentially cause damage and lead to a shortened life cycle of components. The fracture propagation associated with the stress waves is particularly critical for the lightweight composite-overwrapped cylinders because of the low shear and tensile strength at the interface of multimaterial construction and thermal degradation and loading rate dependence in polymer metrix composite material properties. The dynamic analysis is important in highlighting the potential shortcomings of traditional static analyses commonly used in gun tube and piping system design, especially with the goal of achieving a lightweight design. In order to develop a safe, optimum design, this dynamic amplification effect and fracture mechanism must be included in design processes.

5. References

1. Rice, J. R. "A Path Independent Integral and the Approximate Analysis of Strain Concentration by Notches and Cracks." *Journal of Applied Mechanics*, pp. 379–386, June 1968.

2. Taylor, G. I. "Strains in a Gun Barrel Near the Driving Barrel of a Moving Projectile." A.C. 1851/Gn. 104, UK Ministry of Supply, London, England, March 1942.

3. Jones, J. P. and P. G. Bhuta. "Response of Cylindrical Shell to Moving Loads." *Journal of Applied Mechanics Transactions*, vol. 31, no. 86, series E, pp. 105–111, American Society of Mechanical Engineering, March 1964.

4. Tang, S. "Dynamic Response of a Tube Under Moving Pressure." *Journal of the Engineering Mechanics Division Proceedings of the American Society of Civil Engineering*, pp. 97–122, October 1965.

5. Reismann, H. "Response of a Prestressed Cylindrical Shell to Moving Pressure Load, Development in Mechanics." *Solid Mechanics - Preceedings of the Eighth Midwestern Mechanics Conference, Part II*, vol.2, pp. 349–363, Pergamon Press, 1965.

6. Simkins, T. E. "Response of Flexural Waves in Gun Tubes." ARCCB-TR-87008, U.S. Army Research, Development, and Engineering Center, Benet Weapons Laboratory, Watervliet, NY, July 1987.

7. Hopkins, D. A. "Predicting Dynamic Strain Amplification by Coupling a Finite Element Structural Analysis Code with a Gun Interior Ballistic Code." BRL-TR-3269, U.S. Army Ballistic Research Laboratory, Aberdeen Proving Ground, MD, September 1991.

8. Tzeng, J. T. and D. A. Hopkins. "Dynamic Response of Composite Cylinders Subjected to a Moving Internal Pressure." *Journal of Reinforced Plastics and Composites*, vol. 15, no. 11, pp. 1088–1105, November 1996.

9. Halliquist, J. O. "User Manual for DYNA2D - An Explicit Two-Dimensional Hydrodynamic Finite Element Code With Interactive Rezoning and Graphical Display." Lawrence Livermore National Laboratory, 1987.

10. Atluri, S. N. *Computational Methods in Mechanics of Fracture*. Chapter 5, Speringer - Verlag, NY, 1985.

11. Doyle, J. F., and T. N. Farris. "Interaction of Longitudinal Waves With a Lengthwise Crack in a Beam." *ESM Proceedings*, pp. 1253–1260, Portland, June 1988.

12. Alexander, A., and J. T. Tzeng. "Effective Properties of 3D Laminated Composites for Finite Element Applications." *Proceedings of 1994 International Conference of Computer in Engineering*, vol. 2, pp. 507–518, American Society of Mechanical Engineering, 1994.

NO. OF COPIES	ORGANIZATION
2	DEFENSE TECHNICAL INFORMATION CENTER DTIC DDA 8725 JOHN J KINGMAN RD STE 0944 FT BELVOIR VA 22060-6218
1	HQDA DAMO FDQ D SCHMIDT 400 ARMY PENTAGON WASHINGTON DC 20310-0460
1	OSD OUSD(A&T)/ODDDR&E(R) R J TREW THE PENTAGON WASHINGTON DC 20301-7100
1	DPTY CG FOR RDE HQ US ARMY MATERIEL CMD AMCRD MG CALDWELL 5001 EISENHOWER AVE ALEXANDRIA VA 22333-0001
1	INST FOR ADVNCD TCHNLGY THE UNIV OF TEXAS AT AUSTIN PO BOX 202797 AUSTIN TX 78720-2797
1	DARPA B KASPAR 3701 N FAIRFAX DR ARLINGTON VA 22203-1714
1	NAVAL SURFACE WARFARE CTR CODE B07 J PENNELLA 17320 DAHLGREN RD BLDG 1470 RM 1101 DAHLGREN VA 22448-5100
1	US MILITARY ACADEMY MATH SCI CTR OF EXCELLENCE DEPT OF MATHEMATICAL SCI MAJ M D PHILLIPS THAYER HALL WEST POINT NY 10996-1786

NO. OF COPIES	ORGANIZATION
1	DIRECTOR US ARMY RESEARCH LAB AMSRL D R W WHALIN 2800 POWDER MILL RD ADELPHI MD 20783-1145
1	DIRECTOR US ARMY RESEARCH LAB AMSRL DD J J ROCCHIO 2800 POWDER MILL RD ADELPHI MD 20783-1145
1	DIRECTOR US ARMY RESEARCH LAB AMSRL CS AS (RECORDS MGMT) 2800 POWDER MILL RD ADELPHI MD 20783-1145
3	DIRECTOR US ARMY RESEARCH LAB AMSRL CI LL 2800 POWDER MILL RD ADELPHI MD 20783-1145
	ABERDEEN PROVING GROUND
4	DIR USARL AMSRL CI LP (305)

NO. OF COPIES	ORGANIZATION
1	DFNS NUCLEAR AGNCY INVTV CNCPTS DIV JYUJI D HEWITT 6801 TELEGRAPH RD ALEXANDRIA VA 22310-3398
2	PEO ARMAMENTS SFAE AR PM D ADAMS T MCWILLIAMS PICATINNY ARSENAL NJ 07806-5000
1	PEO FAS SFAE FAS PM H GOLDMAN PICATINNY ARSENAL NJ 07806-5000
4	PM CRUSADER G DELCOCO D ELLIS B MACHAK J SHIELDS PICATINNY ARSENAL NJ 07806-5000
2	PM SADARM SFAE FAS SD PICATINNY ARSENAL NJ 07806-5000
4	PM TMAS SFAE AR TMA COL PAWLICKI K KIMKER SFAE AR TMA MD R KOWALSKI SFAE AR TMA MS D GUZIEWICZ PICATINNY ARSENAL NJ 07806-5000
2	DIR USARL AMSRL SE L D SNIDER AMSRL SE L D WOODBURY 2800 POWDER MILL RD ADELPHI MD 20783-1197
1	CDR US ARMY ARDEC F MCLAUGHLIN PICATINNY ARSENAL NJ 07806-5000

NO. OF COPIES	ORGANIZATION
1	CDR US ARMY ARDEC AMSMC PBM K PICATINNY ARSENAL NJ 07806-5000
2	CDR US ARMY ARDEC AMSTA AR CC J HEDDERICH COL SINCLAIR PICATINNY ARSENAL NJ 07806-5000
1	CDR US ARMY ARDEC AMSTA AR CCH PICATINNY ARSENAL NJ 07806-5000
1	CDR US ARMY ARDEC AMSTA AR CCH P J LUTZ PICATINNY ARSENAL NJ 07806-5000
4	CDR US ARMY ARDEC AMSTA AR CCH T R CARR P CHRISTIAN N KRASNOW S MUSALLI PICATINNY ARSENAL NJ 07806-5000
1	CDR US ARMY ARDEC AMSTA AR CCH V E FENNELL PICATINNY ARSENAL NJ 07806-5000
2	CDR US ARMY ARDEC AMSTA AR FSA M D DEMELLA F DIORIO PICATINNY ARSENAL NJ 07806-5000
2	CDR US ARMY ARDEC AMSTA AR TD V LINDNER T PRICE C SPINELLI PICATINNY ARSENAL NJ 07806-5000

NO. OF COPIES	ORGANIZATION
1	CDR USA BELVOIR RD&E CTR STRBE JBC FT BELVOIR VA 22060-5605
4	CDR US ARMY MICOM AMSMI RD W MCCORKLE AMSMI RD ST P DOYLE AMSMI RD ST CN T VANDIVER AMSMI RD ST WF M COLE REDSTONE ARSENAL AL 35898
3	CDR WATERVLIET ARS SMCWV QAE Q C HOWD SMCWV QA QS K INSCO SMCWV SPM T MCCLOSKEY B25 3 WATERVLIET NY 12189-4050
5	DIR ARO G ANDERSON J CHANG A CROWSON K IYER R SINGLETON PO BOX 12211 RESEARCH TRIANGLE PARK NC 27709-2211
10	DIR BENET LABS AMSTA AR CCB G D'ANDREA K MINOR J KEANE J BATTAGLIA J VASILAKIS G FRIAR V MONTVORI J WRZOCHALSKI R HASENBEIN AMSTA AR CCB R S SOPOK WATERVLIET NY 12189-4050
1	DIR USA CRREL P DUTTA 72 LYME RD HANOVER NH 03755
1	DIR DARPA M FREEMAN 3701 N FAIRFAX DR ARLINGTON VA 22203-1714

NO. OF COPIES	ORGANIZATION
1	EXPDTNRY WF DIV N85 F SHOUP 2000 NAVY PENTAGON WASHINGTON DC 20350-2000
2	OFC OF NAVAL RSRCH MECH DIV CODE 1132SM Y RAJAPAKSE D SIEGEL 351 800 N QUINCY ST ARLINGTON VA 22217
1	DAVID TAYLOR RSRCH CTR SHIP STRCTRS & PRTCTN DEPT J CORRADO CODE 1702 BETHESDA MD 20084
1	DAVID TAYLOR RSRCH CTR R ROCKWELL BETHESDA MD 20054-5000
1	NAVAL ORD STN ADVNCD SYS TECH BR D HOLMES CODE 2011 LOUISVILLE KY 40214-5245
1	CDR NSSC D LIESE 2531 JEFFERSON DVS HWY ARLINGTON VA 22242-5160
5	CDR NSWC CODE D4 M E LACY CODE G30 J H FRANCIS CODE G33 J FRAYSSE G GRAFF R HUBBARD DAHLGREN VA 22448
1	CDR NSWC CRANE DIV CODE 20HR M JOHNSON LOUISVILLE KY 40214-5245
2	CDR WRIGHT PTRSN AFB WL FIV A MAYER WL MLBM S DONALDSON 2941 P STREET STE 1 DAYTON OH 45433

NO. OF COPIES	ORGANIZATION
2	NASA LANGLEY RSRCH STR MS 266 AMSRL VS W ELBER AMSRL VS S F BARTLETT JR HAMPTON VA 23681-0001
1	ARGONNE NTNL LAB J M KRAMER 9700 SO CASS AVE ER 207 ARGONNA IL 60439-4841
1	BATTELLE M SMITH PO BOX 999 RICHLAND WA 99352
7	DIR LLNL R CHRISTENSEN S DETERESA S GROVES W FENG A HOLT M FINGER F MAGNESS PO BOX 808 LIVERMORE CA 94550
1	OAK RIDGE NTNL LAB R M DAVIS PO BOX 2008 OAK RIDGE TN 37831-6195
4	DIR SNL APLD MCHNCS DPT DIV 8241 D DAWSON W KAWAHARA P NIELAN K PERANO PO BOX 969 LIVERMORE CA 94550-0096
3	INST FOR ADVNCD TECH H FAIR I MCNAB P SULLIVAN 4030 2 W BRAKER LN AUSTIN TX 78759

NO. OF COPIES	ORGANIZATION
1	NASA LEWIS RSRCH CTR C C CHAMIS 21000 BROOKPARK RD CLEVELAND OH 44135
1	NAVAL SEA SYSTEMS CMD GENE CAMPONESCHI NAVSEA 03 R11 2531 JEFFERSON DAVIS HWY ARLINGTON VA 22242-5160
1	DIR NIST PLYMR DIV PHYMRS RM A209 G MCKENNA GAITHERSBURG MD 20899
1	DIR NIST POLYMER DIV D HUNSTON BLDG 224 GAITHERSBURG MD 20899
1	DIR NIST BUILDING & FIRE RSRCH LAB JOHNNE CHIN GAITHERSBURG MD 20899
1	WILLIAM & MARY COLLEGE DEPT OF APPLIED SCIENCE R PIPES WILLIAMSBURG VA
1	DREXEL UNIV ALBERT S D WANG 32ND & CHESTNUT STS PHILADELPHIA PA 19104
1	PURDUE UNIV SCHOOL OF AERO & ASTRO C T SUN W LAFAYETTE IN 47907-1282
2	STANFORD UNIV DEPT OF ARNTCS & AIRBLSTS S TSAI G SPRINGER STANFORD CA 94305

NO. OF COPIES	ORGANIZATION
2	UNIV OF IL AT URBANA CHAMPAIGN NATL CTR FOR COMPOSITE MATERIALS RSRCH H HILTON J ECONOMY 104 S WRIGHT ST URBANA IL 61801
1	UNIV OF KY LYNN PENN 763 ANDERSON HALL LEXINGTON KY 40506-0046
1	UNIV OF UT MCHNCL & INDSTRL ENGRNG DEPT S SWANSON SALT LAKE CITY UT 84112
3	VA POLY INST & ST UNIV DEPT OF ESM MICHAEL W HYER KENNETH L REIFSNIDER ALFRED LOOS BLACKSBURG VA 24061-0219
1	UNIV OF CA LA MANE DEPT ENGRNG IV H T HAHN LOS ANGELES CA 90024-1597
2	UNIV OF DAYTON RSRCH INST R Y KIM A K ROY 300 COLLEGE PARK AVE DAYTON OH 45469-0168
1	UNIV OF DE CTR FOR CMPST MATLS J GILLESPE 201 SPENCER LAB NEWARK DE 19716
1	UNIV OF MD DEPT OF AEROSPC ENGRNG A J VIZZINI COLLEGE PARK MD 20742

NO. OF COPIES	ORGANIZATION
1	UNIV OF NY AT BUFFALO DEPT OF ELCTRCL ENGRNG J SARJEANT BOX 601900 BUFFALO NY 14260-1900
4	UNIV OF TX AT AUSTIN CTR FOR ELCTRMCHNCS J KITZMILER J PRICE R THOMPSON A WALLS 10100 BURNET RD AUSTIN TX 78758-4497
1	US MILITARY ACDMY DEPT OF CVL & MCHNCL RSRCH LABS J TROVILLION PO BOX 9005 CHAMPAIGN IL 61826-9005
1	AAI CORP TECH LIB PO BOX 126 HUNT VALLEY MD 21030-0126
2	ADVNCD CMPST MATLS CORP R HOOD J RHODES 1525 S BUNCOMBE RD GREER SC 29651-9208
3	ALLIANT TECHSYS INC J BODE C CANDLAND K WARD 5901 LINCOLN DR MINNEAPOLIS MN 55346-1674
1	ALLIANT TECHSYS INC T HOLMQUIST 600 SECOND ST NE HOPKINS MN 55343
1	AMOCO PRFRMNC PRODUCTS M MICHNO JR 4500 MCGINNIS FERRY RD ALPHARETTA GA 30202-3944

NO. OF COPIES	ORGANIZATION
1	APPLIED COMPOSITES W GRISCH 333 NO SIXTH ST ST CHARLES IL 60174
1	BRUNSWICK DFNS T HARRIS 174 JFRSN DVS HWY STE 410 ARLINGTON VA 22202
1	CSTM ANLYTCL ENGRNG SYS INC A ALEXANDER STAR RT BOX 4A FLINTSTONE MD 21530
3	ALLIANT TECHSYSTEMS R BOE J POESCH F POLICELLI PO BOX 98 MAGNA UT 84044
1	HEXCEL M SHELENDICH 11555 DUBLIN BLVD PO BOX 2312 DUBLIN CA 94568-0705
1	IAP RSRCH INC A CHALLITA 2763 CULVER AVE DAYTON OH 45429
1	INTGRTD CMPST TECH H PERKINSON JR PO BOX 397 YORK NEW SALEM PA 17371-0397
1	INTERFEROMETRICS INC R LARRIVA VP 8150 LESSBURG PIKE VIENNA VA 22100
1	KAMAN SCNCS CORP T HAYDEN PO BOX 7463 COLORADO SPRINGS CO 80933

NO. OF COPIES	ORGANIZATION
2	LORAL VOUGHT SYS K COOK G JACKSON 1701 W MARSHALL DR GRAND PRAIRIE TX 75051
2	LOCKHEED MARTIN P DEWAR L SPONAR 230 E GODDARD BLVD KING OF PRUSSIA PA 19406
1	NOESIS INC A BOUTZ 1500 WILSON BLVD STE 1224 ARLINGTON VA 22209
2	PRIMEX TECH FLNCHBGH DIV E STEINER B STEWART PO BOX 127 RED LION PA 17356
1	PRIMEX TECH L WHITMORE 10101 9TH ST N ST PETERSBURG FL 33702
4	DIR US ARMY RESEARCH LAB AMSRL WM MB A ABRAHAMIAN M BERMAN T LI A FRYDMAN 2800 POWDER MILL RD ADELPHI MD 20783-1197

NO. OF COPIES	ORGANIZATION
	ABERDEEN PROVING GROUND
38	DIR USARL AMSRL WM I MAY L JOHNSON AMSRL WM M J MCAULEY D VIECHNICKI G HAGNAUER AMSRL WM B A HORST E SCHMIDT H ROGERS AMSRL WM BC P PLOSTINS J NEWILL S WILKERSON D LYON AMSRL WM MB W SPURGEON S GHIORSE P DEHMER P BLANAS D SPAGNUOLO R KLINGER E RIGAS J BENDER L BURTON B BURNS W DRYSDALE D GRANVILLE D HOPKINS D HENRY C HOPPEL R KASTE J TZENG B FINK T BOGETTI AMSRL WM T W F MORRISON AMSRL WM TA W BUCHEY W GILLICH T HAVEL AMSRL WM TC R COATES W DE ROSSET

NO. OF COPIES	ORGANIZATION
	AMSRL WM BB T HAUG

REPORT DOCUMENTATION PAGE

Form Approved
OMB No. 0704-0188

1. AGENCY USE ONLY *(Leave blank)*	2. REPORT DATE	3. REPORT TYPE AND DATES COVERED
	January 1999	Final, Oct 96 - Jan 98

4. TITLE AND SUBTITLE

Dynamic Fracture of Composite Gun Tubes

5. FUNDING NUMBERS

622618AH80
Navy: R119115WPRS

6. AUTHOR(S)

Jerome T. Tzeng

7. PERFORMING ORGANIZATION NAME(S) AND ADDRESS(ES)

U.S. Army Research Laboratory
ATTN: AMSRL-WM-MB
Aberdeen Proving Ground, MD 21005-5069

8. PERFORMING ORGANIZATION REPORT NUMBER

ARL-TR-1869

9. SPONSORING/MONITORING AGENCY NAMES(S) AND ADDRESS(ES)

U.S. Naval Surface Warfare Center
Dahlgren, VA 22448-9999

10. SPONSORING/MONITORING AGENCY REPORT NUMBER

11. SUPPLEMENTARY NOTES

12a. DISTRIBUTION/AVAILABILITY STATEMENT

Approved for public release; distribution is unlimited.

12b. DISTRIBUTION CODE

13. ABSTRACT *(Maximum 200 words)*

The fracture behavior of a composite cylinder subjected to a moving pressure has been investigated. The resonance of stress waves can result in very high amplitude of strains in the cylinder at the instant and location of pressure front passage when the velocity of the moving pressure approaches a critical velocity. The stress wave with high magnitude, while short in duration, might not cause structural failure immediately; however, it could accelerate the propagation in the cylinder with initial imperfection and shorten fatigue life of the cylinders. The fracture mechanism induced by dynamic amplification effects is especially critical for composite-overwrapped cylinders because of the multimaterial and anisotropic construction, thermal degradation in material properties, and a design goal that is inherent in lightweight gun barrel applications.

14. SUBJECT TERMS

composite, fracture, fatigue, dynamics

15. NUMBER OF PAGES

41

16. PRICE CODE

17. SECURITY CLASSIFICATION OF REPORT	18. SECURITY CLASSIFICATION OF THIS PAGE	19. SECURITY CLASSIFICATION OF ABSTRACT	20. LIMITATION OF ABSTRACT
UNCLASSIFIED	UNCLASSIFIED	UNCLASSIFIED	UL

NSN 7540-01-280-5500

Standard Form 298 (Rev. 2-89)
Prescribed by ANSI Std. 239-18 298-102

USER EVALUATION SHEET/CHANGE OF ADDRESS

This Laboratory undertakes a continuing effort to improve the quality of the reports it publishes. Your comments/answers to the items/questions below will aid us in our efforts.

1. ARL Report Number/Author ARL-TR-1869 (Tzeng) Date of Report January 1999

2. Date Report Received ____________

3. Does this report satisfy a need? (Comment on purpose, related project, or other area of interest for which the report will be used.) ____________

4. Specifically, how is the report being used? (Information source, design data, procedure, source of ideas, etc.) ____________

5. Has the information in this report led to any quantitative savings as far as man-hours or dollars saved, operating costs avoided, or efficiencies achieved, etc? If so, please elaborate. ____________

6. General Comments. What do you think should be changed to improve future reports? (Indicate changes to organization, technical content, format, etc.) ____________

CURRENT ADDRESS

Organization

Name E-mail Name

Street or P.O. Box No.

City, State, Zip Code

7. If indicating a Change of Address or Address Correction, please provide the Current or Correct address above and the Old or Incorrect address below.

OLD ADDRESS

Organization

Name

Street or P.O. Box No.

City, State, Zip Code

(Remove this sheet, fold as indicated, tape closed, and mail.)

(DO NOT STAPLE)

DEPARTMENT OF THE ARMY

OFFICIAL BUSINESS

NO POSTAGE
NECESSARY
IF MAILED
IN THE
UNITED STATES

BUSINESS REPLY MAIL
FIRST CLASS PERMIT NO 0001,APG,MD

POSTAGE WILL BE PAID BY ADDRESSEE

DIRECTOR
US ARMY RESEARCH LABORATORY
ATTN AMSRL WM MB
ABERDEEN PROVING GROUND MD 21005-5069